(to be published in AJ, May 2004)

A Very Large Array 3.6 cm continuum survey of Galactic Wolf-Rayet stars

C. Cappa[1]

Instituto Argentino de Radioastronomía, CC 5, 1894 Villa Elisa, Argentina,
and
Facultad de Ciencias Astronómicas y Geofísicas, Universidad Nacional de La Plata,
Paseo del Bosque s/n, 1900 La Plata, Argentina

ccappa@fcaglp.fcaglp.unlp.edu.ar

W.M. Goss

National Radio Astronomy Observatory,
P.O. Box 0, Socorro, NM 87801, USA

mgoss@aoc.nrao.edu

and

K.A. van der Hucht

SRON National Institute for Space Research
Sorbonnelaan 2, Utrecht, NL-3584 CA, the Netherlands

k.a.van.der.hucht@sron.nl

ABSTRACT

We report the results of a survey of radio continuum emission of Galactic Wolf-Rayet stars north of $\delta = -46°$. The observations were obtained at 8.46 GHz (3.6 cm) using the Very Large Array (VLA), with an angular resolution of $\sim 6'' \times 9''$ and typical rms noise of ~ 0.04 mJy beam^{-1}. Our survey of 34 WR stars resulted in 15 definite and 5 probable detections, 13 of these for the first time at radio wavelengths. All detections are unresolved ($\theta \lesssim 5''$). Time variations in flux are confirmed in the cases of WR 98a, WR 104, WR 105, and WR 125. WR 79a and WR 89 are also variable in flux and we suspect they are also non-thermal emitters. Thus, of our sample 20 - 30 % of the detected stars are non-thermal emiters. Average mass loss rates determinations obtained excluding definite and suspected non-thermal cases give similar values for

[1]Member of Carrera del Investigador Científico, CONICET, Argentina

WN (all subtypes) and WC5-7 stars ($\dot{M}$(WN) = [4 ± 3]×10^{-5} M$_\odot$ yr^{-1} and $\dot{M}$(WC5-7) = [4 ± 2]×10^{-5} M$_\odot$ yr^{-1}), while a lower value was obtained for WC8-9 stars ($\dot{M}$(WC8-9) = [2 ± 1]×10^{-5} M$_\odot$ yr^{-1}). Uncertainties in stellar distances largely contribute to the observed scatter in mass loss rates. Upper limits to the mass loss rates were obtained in cases of undetected sources or for sources which probably show additional non-thermal emission.

Subject headings: radio continuum: stars; — stars: mass loss; — stars: Wolf-Rayet

1. Introduction

Wolf-Rayet (WR) stars are the evolved descendants of massive O-type progenitors ($M_{\rm i} > 22\,{\rm M}_\odot$) and are considered to be the immediate precursors of supernovae Type Ib and Type Ic (e.g., Maeder 1981; Meynet & Maeder 2003). They are characterized by powerful stellar winds with terminal velocities $v_\infty \simeq 400\,\text{-}\,5500\,{\rm km\,s^{-1}}$ (e.g., Prinja et al. 1990; Eenens & Williams 1994; Kingsburgh et al. 1995; for an overview see van der Hucht 2001, table 15, column 14), and mass loss rates in the range (1 - 5)×10^{-5} M$_\odot$ yr^{-1} (e.g., Abbott et al. 1986 [hereafter AB86]; Leitherer et al. 1995, 1997 [hereafter LC95, LC97]; Chapman et al. 1999 [hereafter CL99]). Due to these properties WR stars are not only interesting in themselves, but also important species for chemical enrichment and galactic evolution (e.g., Dray et al. 2003; De Donder & Vanbeveren 2003). For general reviews of the WR phenomenon, see, e.g., van der Hucht (1992) and Maeder & Conti (1994).

The strong stellar winds of WR stars reveal themselves in the electromagnetic spectrum from the UV (P-Cygni profiles of resonance lines) to the IR/radio range (free-free radiation). Therefore, an important diagnostic tool to obtain information about stellar wind properties of massive stars is the study of the radio continuum emission from their close environs. Radio observations provide a reliable method for determining stellar mass loss rates if the emission is thermal in origin, since the measured radio flux density is related to the mass loss rate by an analytical expression (e.g., Wright & Barlow 1975; Panagia & Felli 1975). This emission is the free-free radiation originating in the ionized wind, expanding at constant velocity. It arises from the outer parts of the wind envelope and is partially optically thick in the radio region, showing positive spectral indices ($\alpha \geq +0.6$, where $S_\nu \propto \nu^\alpha$).

However, the last decade has seen an increasing number of discoveries of WR stars with non-thermal radio emission in addition to their free-free emission. Non-thermal emission is thought to be produced by electrons accelerated in strong shocks in the winds of single stars (White 1985) or in the shocked wind-wind collision region between massive WR+O binaries (e.g., Williams et al. 1990; Eichler & Usov 1993). Unlike thermal emission, non-thermal emission has a negative spectral index and can be variable. Van der Hucht et al. (1992) suggested that all cases of WR non-thermal radio emission correspond to WR+OB colliding wind binaries, which has been corroborated by Dougherty & Williams (2000).

Due to their relatively large distances (van der Hucht 2001), the number of WR radio continuum detections was limited to only about 44 cases (AB86, LC95, LC97 and CL99). The VLA survey by AB86, which also quotes previous observations, contains radio data for 40 WR stars at $\delta > -47°$ with 27 detections using the VLA, with rms noise values of 0.06 - 0.23 mJy beam^{-1}. They found 77% probable or definite thermal wind sources and 12% probable or definite non-thermal sources. In the southern hemisphere, LC95, LC97 and CL99 surveyed 36 WR stars ($\delta < -45°$) at two frequencies using the ATCA, with rms noise values of 0.10 - 0.15 mJy beam^{-1}. Other WR radio continuum studies have been performed for WR 140 by Williams et al. (1987, 1990, 1994) and White & Becker (1995); for WR 146 by Dougherty et al. (1996, 2000) and Setia Gunawan et al. (2000); for WR 147 by Moran et al. (1989), Churchwell et al. (1992), Davis et al. (1996), Williams et al. (1997), Skinner et al. (1999), Setia Gunawan et al. (2001), Watson et al. (2002) and Dougherty et al. (2003); for Galactic Center WR stars by Lang et al. (2001) and Lang (2003); for WR 98a, WR 104 and WR 112 by Monnier et al. (2002); and for massive stars in Cyg OB2 by Setia Gunawan et al. (2003b). In these studies, some 70 out of the $\sim$250 known Galactic WR stars (van der Hucht 2001, 2003) have been investigated for radio continuum emission, resulting into 44 positive detections. The ATCA survey also indicates that at least 40% of the WR stars with measured radio spectral indices contain a non-thermal component at centimeter wavelengths, a percentage that, coincidentally, is equal to the percentage of WR+OB binaries among the known Galactic WR stars (van der Hucht 2001).

In this paper we report on the results of a survey of radio continuum emission from Galactic WR stars at 3.6 cm with higher sensitivity than available before. Our aim is to increase the sample of WR stars with radio continuum observations in order to derive mass loss rates or upper limits, and to identify non-thermal cases. As a first step, we performed observations at one frequency only. Consequently, spectral indices of detected sources can only be determined here using radio data at other wavelengths from the literature and may be influenced by variability. Thus, new radio continuum observations are important to find new thermal and non-thermal WR radio sources, the thermal ones providing mass loss rates, crucial for testing existing wind models, and the non-thermal ones pointing to colliding winds in WR+OB binaries.

2. Selected Wolf-Rayet stars

In order to achieve these goals, we selected 33 WR stars from the catalog by van der Hucht (2001). To select the targets, we took into account all WR stars north of $\delta = -46°$, and selected the ones with expected free-free flux densities $S_{\rm exp} > 0.075$ mJy. $S_{\rm exp}$ was determined with the classical expressions by Panagia & Felli (1975) and Wright & Barlow (1975) for the radio emission from an optically thick stellar wind flowing at constant velocity. In order to estimate these values, we adopt for all sources the same mass loss rate $\dot{M} = (1.5\text{ - }2.0)\times10^{-5}\ {\rm M_\odot\ yr^{-1}}$, and stellar distances and terminal velocities from van der Hucht (2001).

With these assumptions, we found $S_{\rm exp} > 0.075$ mJy for 64 WR stars. Only 27 of these stars had previous radio detections, and radio flux density upper limits were available for 12 stars. We

were then left with 37 stars which either had not been observed yet or had not been detected. We selected 26 of these stars as our targets, listed in Table 1. In our sample we included some WR stars previously detected: WR 79a (HD 152804, detected with the VLA by Bieging et al. 1989), WR 81, WR 89, WR 98a, WR 104, WR 105, and WR 125. The detection of WR 81 by AB86 was doubtful. WR 98a, WR 104, WR 105 and WR 125 are known non-thermal emitters and, thus, may vary in flux density.

TABLE 1

In order to find new non-thermal candidates, we included binaries and suspected binaries listed by van der Hucht et al. (2001). About 70% of the stars are closer than 3.0 kpc, while no stars beyond 5.3 kpc are included.

3. VLA observations

We performed radio continuum observations at 8.46 GHz with the VLA in the direction of the selected WR stars. Thirty-three fields were observed on 15 September 2001 (during the move from the C- to the DnC-array), 5 and 8 October 2001 (in the DnC-array) and 12 November 2001 (in the D-array). With the exception of WR 89, the field centers coincide with the stellar positions. The bandwidth was 50 MHz. The on-source observing time was about 25 minutes for each field to achieve a rms noise of $\sim$0.04 mJy beam^{-1}. The synthesized beam is about $6''.1\times9''.0$ in all cases.

The data were edited, calibrated and imaged following a standard way using AIPS tasks. After editing, the data were calibrated both in amplitude and phase. The primary flux density calibrators were 3C 48 and 3C 286. We used phase referencing taking into account a selection of nearby point sources with precision positions ($0''.1$ or better). The secondary calibrators were 0244+624, 0747–331, 0828–375, 1001–446, 1604–446, 1744–312, 1751–253, 1820–254, 1832–105, 1851+005, 1924+156, 2015+371, 2230+697 and 2250+558. The fields corresponding to WR 4, WR 96 and WR 142 were also self-calibrated in phase, since peak flux densities within the primary beam exceed 10 mJy beam^{-1}. Primary beam correction was applied to the images corresponding to WR 89 and WR 105. WR 89 is in the same field as WR 87, $1'.9$ far from the field center. The primary beam correction factor for WR 89 is 1.5. In the case of WR 105, two additional point-like sources, with no relation to the WR star, are detected close to the center of the field. Diffuse emission from extended sources detected in the fields of WR 87, WR 104, WR 106, WR 113, WR 114, WR 121, WR 125, WR 142, WR 143 and WR 153ab was removed by applying an UV-range ≥ 5Kλ (rejecting spatial scales $\simeq 40''$).

4. Observed radio emission

We report 15 definite and 5 probable detections at 3.6 cm out of the 34 observed WR stars. For 10 out of the 15 definite detections and 3 out of the 5 probable detections this represents a first radio detection, while four definite detections had been previously identified at 3.6 cm and one had been detected previously at a different frequency. All 20 detections are unresolved. The images of the certain and probable detections are displayed in Figs. 1 to 20. The synthesized beam of each field is shown in a corner of the contour plots.

Radio detections with signal-to-noise $S / N \geq 5$, as derived from the Gaussian fitting, and close agreement between radio and optical positions were classified as definite detections, while probable detections correspond to sources with $S / N \approx 4$ (WR 81, WR 95, WR 114 and WR 155) or with relatively large difference between the optical and the radio positions (WR 79a and WR 95). Detections classified as probable need further confirmation.

FIGURES 1 - 20

Flux densities and radio positions were obtained by fitting a 2-D Gaussian with the AIPS-JMFIT tool. In most of the detections, the uncertainty in the radio position is less than $1''$. Except for WR 79a and WR 95, the optical and radio positions agree within $2''$. The flux density uncertainties quoted in the table are equal to the rms noise (1σ) of the images. Flux density uncertainties were derived from the images by taking into account a relatively large region near the detected sources. For the 14 undetected sources, the upper limits in flux density correspond to $3\,\sigma$. Typically, the $1\,\sigma$ level is in the range 0.025 - 0.084 mJy beam^{-1}. In the cases of WR 79a and WR 89, the $1\,\sigma$ level is 0.13 mJy beam^{-1}. The large rms noise associated with the detection of WR 89 is due to the fact that this star is displaced about $1\farcm9$ from the field center. The typical uncertainty in the radio position is $0.5''$.

Table 2 lists the observed 3.6 cm flux densities and radio coordinates of the definite and probable detections, along with the optical coordinates from the catalog of van der Hucht (2001). Non-detected sources are also indicated at the botton of the table. The latter have typical uncertainties of about $1''$ (Leitherer et al. 1997).

TABLE 2

In Table 3, we compare our 3.6 cm detections with previously determined flux densities or upper limits at six radio wavelengths. The table also gives spectral indices α when calculable.

Since we performed observations at one frequency only, spectral indices can not be derived from our data. Thus, the nature of the emission was inferred by comparing the observed fluxes with earlier determinations, allowing us to identify variable sources. Variability in flux density, which is a hint for the presence of non-thermal emission, is also indicated in Table 3.

TABLE 3

5. Comments on individual stars

WR 79a, WN9ha (Fig. 4). This object is a known visual binary with $\Delta\phi = 6''\!.9$ (Mason et al. 1998; van der Hucht 2001, table 22). The radio source extends to the W. The earliest flux density determinations by BA89 (VLA) indicated thermal emission with a spectral index $\alpha = +0.8$. Recent ATCA observations (November 2000) by Setia Gunawan et al. (2003a) show a flat non-thermal energy distribution with spectral index $\alpha = -0.0 \pm 0.1$. Our 3.6 cm observation, less than a year later, is consistent with the ATCA observation and, with respect to BA89 observation, with a variable non-thermal component.

WR 81, WC9 (Fig. 5). Our VLA image shows a source with a complex structure coincident with the optical position of the star. We identified the source to the N as the WR star because of its proximity ($2''\!.5$) to the optical position. The radio source detected by AB86 and identified by these authors as the WR star (see their Fig. 1) is $4''\!.6$ south of the optical position and closer to the southern extension of the radio source detected in the new image. A spectral index cannot be derived.

WR 89, WN8h+OB (Fig. 7). This source was detected in the image corresponding to WR 87, $1'\!.9$ displaced from the field center. Previous flux density determinations by LC95 were consistent with a thermal wind. Judging from our observation, the 3.6 cm flux density dropped some 30 % in recent years. WR 89 is associated with the open cluster Havlen-Moffat No. 1 (C1715−387, Vázquez & Baume 2001).

WR 98a, WC8-9vd+? (Fig. 9). In the infrared this object shows a expanding dust spiral, rotating with a period $P = 565 \pm 50$ d (Monnier et al. 1999), which is considered to be the binary period. Monnier et al. (2002) observed this object with the VLA in 1999.7 and 2000.2 and found the source to be non-thermal. Our 3.6 cm flux density determination is ~ 20 % below their result. Apparently, the non-thermal source is variable.

WR 104, WC9d+B0.5V (Fig. 12). In the infrared this object shows a expanding dust spiral, rotating with a period $P = 243 \pm 3$ d (Tuthill et al. 1999), which is considered to be the binary period. Monnier et al. (2002) found the source to be non-thermal. Our 3.6 cm flux density determination is ~ 40 % below theirs, thus, the non-thermal source is apparently variable.

WR 105, WN9h (Fig. 13). This star shows variable non-thermal flux densities. Our 3.6 cm flux density is $\sim 50\,\%$ larger than the one measured by LC97. The double radio source to the S of the optical position of WR 105 was also detected by AB86 (see their fig. 1). These radio sources were not detected in the NVSS (Condon et al. 1998), nor were optical counterparts found. Zoonematkermani et al. (1990, radio continuum at 20 cm) detected the double source with flux densities of 22 mJy and 16 mJy, while from our VLA data we estimate 6.4 ± 0.2 mJy and 5.4 ± 0.2 mJy. These non-thermal sources have spectral indices α of -0.7 and -0.6, respectively.

WR 125, WC7ed+O9III (Fig. 17). The AB86 1982 observations at 6.3 cm and 2.0 cm showed a non-thermal radio source with $\alpha = -0.5$. Our 2001 3.6 cm flux density observation agrees with the AB86 data for a non-thermal source with that spectral index. The source is variable in flux and turned from non-thermal to thermal in WH92 (see Table 3). We suggest here that the emission is again non-thermal because of the similarity in flux density levels between the AB86 and the present data. The detection of non-thermal emission in 1982 and in 2001 suggests a period of around 20 years. On the other hand, the last IR excess of the WC+O binary WR 125 started in 1991 (WH92), continued till 1993 and then faded away. IR monitoring performed during the last 18 years showed only one period of infrared excess (Williams 2002), implying an orbital period of at least 18 years. WR 125 has much in common with the archetype WR colliding wind binary WR 140 (HD 193793, WC7pd+O4-5, Williams et al. 1990), which has a thermal to non-thermal radio light curve with a period of 7.94 yr (Williams et al. 1994). If WR 125 is an analog of WR 140, then its 1992 IR excess occurred at periastron passage in an eccentric orbit, and an IR excess will happen again in $\sim$2010 - 2012.

WR 133, WN5+O9I (Fig. 18). We detect a double point-like source (separation $\sim 10''$) with the southern component coincident with the optical position of the WN5+O9I binary (Fig. 18, upper panel), which is a known visual binary ($\Delta\phi = 5\farcs4$, Hartkopf et al. 1999; van der Hucht 2001, table 22). The source to the NE has a flux density of $S_{3.6\mathrm{cm}} = 0.39 \pm 0.03$ mJy beam^{-1}. The lower panel of Fig. 18 displays an overlay of the radio continuum emission and the DSS2 red image, suggesting the presence of an additional star NE of the WR system, coincident in position with the northern radio source. Pollock et al. (1995) found a *ROSAT* X-ray excess for WR 133, indicative for a colliding wind binary.

Finally, we note that a radio source with a flux density $S_{3.6cm} = 0.15 \pm 0.04$ mJy is detected $2\farcs5$ far from the optical position of WR 4. We believe that this star has probably been barely detected, but, because of the low S / N ratio and the difference between the optical and radio positions (2.1σ), we have listed this star as non-detected.

In summary, we note that WR 79a, WR 89, WR 98a, WR 104, WR 105 and WR 125 are variable, which can be explained by the presence of a non-thermal component. This implies that our observations of these six stars cannot really be used for mass loss rate determinations, or will yield only upper limits. Of the above six cases all three WCd objects (WR 98a, WR 104 and WR 125) turn out to be variable non-thermal radio sources, suggesting a large number of non-thermal cases

between these objects. Additional observations are necessary to investigate the nature of the other three WCd stars in our sample (WR 95, WR 103 and WR 113) since previous observations only provided upper limits to the flux densities.

6. Radio mass loss rates

Following Panagia & Felli (1975) and Wright & Barlow (1975), the flux density due to thermal *Bremsstrahlung* in an ionized expanding stellar wind can be expressed as

$$S_\nu = 2.32 \times 10^4 (\frac{\dot{M} Z}{v_\infty \mu})^{4/3} (\frac{\gamma g_{\rm ff} \nu}{d^3})^{2/3} \qquad (1),$$

where S_ν is the flux density in mJy, $\dot{M}$ is the mass loss rates in $\mathrm{M_\odot\,yr^{-1}}$, v_∞ is the terminal velocity in $\mathrm{km\,s^{-1}}$, ν is the frequency in Hz and d is the distance in kpc. μ, Z and γ are the mean molecular weight, the rms ionic charge and the mean number of electrons per ion, respectively. This expression corresponds to a spherically symmetric, stationary, isothermal wind flowing at constant velocity. The free-free Gaunt factor $g_{\rm ff}$ can be approximated, following Leitherer & Robert (1991) as

$$g_{\rm ff} = 9.77(1 + 0.13 log \frac{T_{\rm e}^{3/2}}{Z \nu}) \qquad (2).$$

In this expression, $T_{\rm e}$ is the electron temperature of the wind in K.

Based on Equations (1) and (2), we have derived mass loss rates $\dot{M}$ corresponding to the observed flux densities at 3.6 cm, assuming that the observed radio emission is due to free-free emission. In the case of non-thermal contributions, our values represent upper limits to the true mass loss rate. All non-detections are indicated as upper limits to $\dot{M}$. Following LC97, we adopted $T_{\rm e} = 10^4$ K in expression (2). As pointed out by these authors, this temperature has a very minor effect on the $g_{\rm ff}$. Values for the mean molecular weight, the rms ionic charge and the mean number of electrons per ion were taken from LC97. The values adopted for the WO star in our sample, WR 142, are those for the WC4 subtype (Crowther et al. 1998).

Table 4 lists the derived mass loss rates $\dot{M}$ and upper limits. Uncertainties in these values come from several sources. Errors in mass loss rate determinations were estimated following eq. (5) in LC97. We adopted similar criteria as LC97 to estimate the uncertainty in each parameter. For the error in the distances we assumed 20% in case of cluster/associations distances and 50% in case of field stars. The logarithmic uncertainty is then ±0.09 and ±0.25, respectively. Errors in $g_{\rm ff}$ are about 10% (0.05 in logarithmic scale). We adopted uncertainties in wind terminal velocities of 10% (i.e., a logarithmic error of ±0.04). Finally, logarithmic errors in Z, γ and μ were adopted as ±0.08. Typical logarithmic errors in $\log \dot{M}$ are in the range ± 0.20 to ± 0.24 in case of cluster/association

distances and $\pm\,0.40$ in case of field stars. With the quoted uncertainties for the stellar distances and other wind parameters, uncertainties in mass-loss rates determinations are dominated by errors in distances, while uncertainties in flux densities have a minor impact.

TABLE 4

Other sources of error are non-thermal contributions to the flux at 3.6 cm. Inhomogeneities or clumping in the stellar winds lead to over estimates of the final values as emphasized by, e.g., Contreras et al. (1996) and Morris et al. (2000). The latter found volume filling factors of the range 0.04 - 0.25, leading to mass-loss rates a factor of 2.5 - 5 lower than expected for smooth, homogeneous winds. These effects have not been considered here.

7. Discussion

In order to compare mass loss rates derived for different WR subtypes from available radio surveys, we plotted the ATCA and VLA mass loss rates *versus* WR subtype in Fig. 21. The ATCA surveys have been performed by LC95, LC97 and CL99. Previous VLA results were published by Willis (1991) (who updated AB86 results by taking into account new criteria in terminal velocities and in the chemical composition of the region where radio emission originates) and by Monnier et al. (2002).

FIGURE 21

Monnier et al. observed WR 98a and WR 104 at several frequencies and found a non-thermal component in addition to the thermal one. They separated both components and derived a mass-loss rate from the best-fitting value to the thermal emission. The $\dot{M}$-values they derived are 0.8×10^{-5} $M_{\odot}\,yr^{-1}$ for WR 98a and 0.5×10^{-5} $M_{\odot}\,yr^{-1}$ for WR 104.

The upper panel of Fig. 21 displays the mass loss rate (log $\dot{M}$) as a function of the spectral WR subtype for the stars included in our VLA survey. *Bona-fide* mass loss rate estimates are indicated by filled circles, while open circles indicate upper limits both for the variable detected sources and the undetected sources. Uncertainties in the derived values are also indicated. Note that we have plotted the mass loss rates derived by Monnier et al. instead of our estimates listed in Table 4.

The lower panel of Fig. 21 shows all radio mass loss rates from the ATCA and VLA samples. Although more than one mass loss rate determination is available for some of the stars, we plotted

only one value for each star from (in order of preference) Monnier et al. (2002), new VLA data, ATCA data and previous VLA surveys. In the cases of non-thermal sources listed by LC97 and CL99, the $\dot{M}$-values plotted are upper limits. As for the upper panel, open circles indicate upper limits both for undetected sources and variable detected sources.

Excluding definite and suspected non-thermal cases (WR 79a, WR 89 and WR 105) the average mass loss rate for the WN stars detected in our survey is $\dot{M}(\mathrm{WN}) = [4.3 \pm 2.5] \times 10^{-5}\ \mathrm{M}_\odot\ \mathrm{yr}^{-1}$, equal to the average WN mass loss rate in ATCA and previous VLA data sets of $\dot{M}(\mathrm{WN}) = 4 \times 10^{-5}\ \mathrm{M}_\odot\ \mathrm{yr}^{-1}$.

Mass loss rates determined from emission lines studies by Nugis & Lamers (2000) differ from values derived from radio continuum data: in some cases (WR 104 and WR 113), $\dot{M}$ derived from emission lines are factors of two smaller than our radio estimates, while in other cases (WR 81, WR 95 and WR 103) factors of two larger than our results. Clumping and/or an ionization or temperature structure different from our assumptions may account for the differences.

We have thirteen WC8-9 stars included in our sample and detected seven of them. Four of these stars had no radio detections yet (WR 88, WR 95, WR 103 and WR 113), thus increasing to 12 the number of WC8-9 stars with radio detections. Most of these stars have heated circumstellar dust shells (see Williams 1995). WR 95, WR 103 and WR 113 are known to have persistent dust shells (see Table 1). The distribution of these stars in the diagram displays the same trend as in fig. 17 of LC97, with relatively low mass loss rates. The average mass loss rate for WC8-9 stars detected in our sample, excluding definite non-thermal cases (WR 98a and WR 104) is $\dot{M}(\mathrm{WC8\text{-}9}) = [1.7 \pm 1.0] \times 10^{-5}\ \mathrm{M}_\odot\ \mathrm{yr}^{-1}$. The average mass loss rate for WC5-7 stars, obtained from *bona-fide* values from the ATCA (5 stars) and the previous (2 stars) and present (1 star) VLA samples, is $\dot{M}(\mathrm{WC5\text{-}7}) = [4.4 \pm 1.6] \times 10^{-5}\ \mathrm{M}_\odot\ \mathrm{yr}^{-1}$, higher than the value derived for WC8-9 stars. Note, on the other hand, that average values for WN and WC5-7 stars are equal. Uncertainties in stellar distances clearly contribute to the observed scatter of mass loss rates.

The presence of dust in the wind envelopes might decrease the escaping UV photon flux, lowering the thermal radio emission, as suggested by Monnier et al. (2002), and thus the derived mass loss rates. LC97 suggest that this may explain the low mass loss rates obtained for WC9 stars from radio data. Note that the mass loss rates for the WC8 star WR 98a, which also displays a dust persistent shell, is also relatively low (see Fig. 21, lower panel).

The percentage of non-thermal emitters between the detected sources in our sample is 20-30 %. A similar value is derived for the 1986 VLA survey (which includes also previous results). Our percentage is lower than the one derived from ATCA data (40 %).

The case of WR 89 (suggested to be a binary by van der Hucht 2001), which shows time variations in flux density (see Table 3), hints to additional non-thermal emission (the radio spectrum was thermal at the time of the ATCA observations). WR 79a also appears to be variable in flux, suggesting the presence of a non-thermal component. However, a variable thermal component can not be discarded (e.g., Watson et al. 2002). It would be desirable to perform multifrequency radio observations of WR 79a and WR 89 to look for variability and to analyze the nature of the flux

variations.

Finally, we would like to comment on the undetected stars. We repeat here that uncertainties in the expected flux densities $S_{\rm exp}$ are quite large, arising mainly from uncertainties in distances of WR field stars and in the expected range of mass loss rates ($1 - 5\times10^{-5}$ $M_\odot$ yr^{-1}). $S_{\rm exp}$ values for WR 79b, WR 92, WR 96 and WR 119 are 0.12 - 0.26, 0.09 - 0.14, 0.10 - 0.16 and 0.11 - 0.16 mJy, respectively, which are below our detection limit (see Table 2). $S_{\rm exp}$ values were estimated adopting the stellar parameters of Tables 1 and 4, and mass loss rates in the range $(1.5 - 2.0)\times10^{-5}$ $M_\odot$ yr^{-1}. For the cases of WR 80 and WR 121, however, $S_{\rm exp} = 0.5 - 0.8$ and 0.4 - 0.6 mJy, respectively. The derived upper limit is 0.17 mJy (3σ) for both stars. Although a mass loss rate lower than typical can not be discarded, the objects may be at larger distances than adopted here, thus lowering the expected flux density.

8. Conclusions and suggestions for future work

We performed a survey of 34 Galactic Wolf-Rayet stars at 3.6 cm within the declination range of the Very Large Array. We report 15 definite and 5 probable detections. Of these 20 sources, 13 were detected for the first time at radio frequencies.

We confirm time variations in flux of WR 98a, WR 104, WR 105, and WR 125, which support the presence of a non-thermal component. For WR 125 (WC7ed+O9III) we suggest a binary period lower than 20 yr. WR 79a (HD 152408, WN9ha) and WR 89 are also variable in flux and we suspect they are also non-thermal emitters. Non-thermal radiation is indicative for wind-wind collision in WR+OB binaries. Thus, of our sample 20 - 30 % of the detected stars are non-thermal radio sources.

Averages of mass loss rate determinations yield similar values for WN (all subtypes) and WC5-7 stars ($\dot{M}$(WN) = $[4 \pm 3]\times10^{-5}$ $M_\odot$ yr^{-1} and $\dot{M}$(WC5-7) = $[4 \pm 2]\times10^{-5}$ $M_\odot$ yr^{-1}), while a slightly lower value was derived for WC8-9 stars ($\dot{M}$(WC8-9) = $[2 \pm 1]\times10^{-5}$ $M_\odot$ yr^{-1}).

Future observations at several radio frequencies should monitor the objects WR 79a, WR 89, WR 98a, WR 104 and WR 125 during long time periods. These observations can help to determine the presence of non-thermal contributions to the flux density as a function of time. Radio observations at low and high frequencies of the sources first detected will be useful to investigate the nature of the radio emission.

Acknowledgements. We thank the anonymous referee for very helpful comments and suggestions that help to improve the presentation of the paper. C.C. is grateful to the kind hospitality during her stay at AOC, NRAO in Socorro, New Mexico. The National Radio Astronomy Observatory is a facility of the National Science Foundation operated under cooperative agreement by Associated Universities, Inc. This research was partially supported by Facultad de Ciencias As-

tronómicas y Geofísicas, Universidad Nacional de La Plata; project 11/G049 (UNLP); and CONICET project PIP 607/98, Argentina. C.C. acknowledges a travel grant from Fundación Antorchas, Argentina, through project 13622/10.

REFERENCES

Abbott, D.C., Bieging, J.H., Churchwell, E.B., & Torres, A.V. 1986, ApJ, 303, 239 [AB86]

Bieging, J.H., Abbott, D.C., & Churchwell, E.B. 1982, ApJ, 263, 207

Bieging, J.H., Abbott, D.C., & Churchwell, E.B. 1989, ApJ, 340, 518

Chapman, J.M., Leitherer, C., Koribalski, B., Bouter, R., & Storey, M. 1999, ApJ, 518, 890 [CL99]

Churchwell, E.B., Bieging, J.H., van der Hucht, K.A., Williams, P.M., Spoelstra, T.A.Th, & Abbott, D.C. 1992, ApJ, 393, 329

Condon, J.J., Cotton, W.D., Greisen, E.W., Yin, Q.F., Perley, R.A., Taylor, G.B., & Broderick, J.J. 1998, *The NRAO VLA Sky Survey*, AJ, 115, 1693

Contreras, M.E., Rodríguez, L.F., Gomez, Y., & Velázquez, A. 1996, ApJ, 469, 329

Crowther, P.A., De Marco, O., & Barlow, M.J. 1998, MNRAS, 296, 367

Davis, R.J., Bode, M.F., Cohen, R.J., Dougherty, S.M., van der Hucht, K.A., & Williams, P.M. 1996, in: A.R. Taylor & J.M. Paredes (eds.), *Radio Emission from the Stars and the Sun*, ASP-CS 96, 32

De Donder, E., & Vanbeveren, D. 2003, New Astronomy, 8, 415

Dougherty, S.M., Pittard, J.M., Kasian, L., Coker, R.F., Williams, P.M., & Lloyd, H.M. 2003, A&A, 409, 417

Dougherty, S.M., & Williams, P.M. 2000, MNRAS, 319, 1005

Dougherty, S.M., Williams, P.M., & Pollacco, D.L. 2000, MNRAS, 316, 143

Dougherty, S.M., Williams, P.M., van der Hucht, K.A., Bode, M.F., & Davis, R.J. 1996, MNRAS, 280, 963

Dray, L.M., Tout, C.A., Karakas, A.I., & Lattanzio, J.C. 2003, MNRAS, 338, 973

Eenens, P.R.J., & Williams, P.M. 1994, MNRAS, 269, 1082

Eichler, D., & Usov, V. 1993, ApJ, 402, 271

Hartkopf, W.I., Mason, B.D., Gies, D.R., ten Brummelaar, T., McAlister, H.A., Moffat, A.F.J., Shara, M.M., & Wallace, D.J. 1999, AJ118, 509

van der Hucht, K.A., Williams, P.M., Spoelstra, T.A.Th., & de Bruyn, A.G. 1992, in: L. Drissen, C. Leitherer & A. Nota (eds.), *Non-isotropic and Variable Outflows from Stars*, ASP-CS 22, 253

van der Hucht, K.A. 2001, New Astronomy Reviews, 45, 135

van der Hucht, K.A. 2003, in: K.A. van der Hucht, A. Herrero & C. Esteban (eds.), *A Massive Star Odyssey, from Main Sequence to Supernova*, Proc. IAU Symp. No. 212 (San Francisco: ASP), p. 441

Kingsburgh, R.L., Barlow, M.J., & Storey, P.J. 1995, A&A, 295, 75

Lang, C.C., Goss, W.M., & Rodríguez, L.F. 2001, ApJ, 551, L143

Lang, C.C. 2003, in: K.A. van der Hucht, A. Herrero & C. Esteban (eds.), *A Massive Star Odyssey, from Main Sequence to Supernova*, Proc. IAU Symp. No. 212 (San Francisco: ASP), p. 497

Leitherer, C., & Robert, C. 1991, ApJ, 377, 629

Leitherer, C., Chapman, J.M., & Koribalski, B. 1995, ApJ, 450, 289 [LC95]

Leitherer, C., Chapman, J.M., & Koribalski, B. 1997, ApJ, 481, 898 [LC97]

Maeder, A. 1981, A&A, 99, 97

Maeder, A., & Conti, P.S. 1994, ARA&A, 32, 227

Mason, B.D., Gies, D.R., Hartkopf, W.I., Bagnuolo, W.G., den Brummelaar, T., & McAlister, H.A. 1998, AJ115, 821

Meynet, A., & Maeder, A. 2003, A&A, 404, 975

Monnier, J.D., Tuthill, P.G., & Danchi, W.C. 1999, ApJ, 525, L97

Monnier, J.D., Greenhill, L.J., Tuthill, P.G., & Danchi, W.C. 2002, ApJ, 566, 399

Moran,J.P., Davis, R.J., Bode, M.F., Taylor, A.R., Spencer, R.E., Argue, A.N., Irwin, M.J., & Shanklin, J.D. 1989, Nature, 340, 449

Morris, P.M., van der Hucht, K.A., Crowther, P.A., Hillier, D.J., Dessart, L., Williams, P.M., & Willis, A.J. 2000, A&A, 353, 624

Nugis, T., & Lamers, H. 2000, A&A, 360, 227

Panagia, N., & Felli, M. 1975, A&A, 39, 1

Pollock, A.M.T., Haberl, F., & Corcoran, M.F. 1995, in: K.A. van der Hucht & P.M. Williams (eds.), *Wolf-Rayet Stars: Binaries, Colliding Winds, Evolution*, Proc. IAU Symp. No. 163 (Dordrecht: Kluwer), p. 512

Prinja, R.K., Barlow, M.J., & Howarth, I.D. 1990 ApJ, 361, 607 (Erratum 1991, ApJ, 383, 466)

Setia Gunawan, D.Y.A., de Bruyn, A.G., van der Hucht, K.A., & Williams, P.M. 2000, A&A, 368, 484

Setia Gunawan, D.Y.A., de Bruyn, A.G., van der Hucht, K.A., & Williams, P.M. 2001, A&A, 356, 676

Setia Gunawan, D.Y.A., Chapman, J.M., Stevens, I.R., Rauw, G., & Leitherer, C. 2003a, in: K.A. van der Hucht, A. Herrero & C. Esteban (eds.), *A Massive Star Odyssey, from Main Sequence to Supernova*, Proc. IAU Symp. No. 212 (San Francisco: ASP), p. 230

Setia Gunawan, D.Y.A., de Bruyn, A.G., van der Hucht, K.A., & Williams, P.M. 2003b, ApJS, 149, 123

Skinner, S.L., Itoh, M., Nagase, F., & Zhekov, S.A. 1999, ApJ, 524, 394

Tuthill, P.G., Monnier, J.D., & Danchi, W.C. 1999, Nature, 398, 487

Vázquez, R.A., & Baume, G. 2001, A&A, 371, 908

Watson, S.K., Davis, R.J., Williams, P.M., & Bode, M.F. 2002, MNRAS, 334, 631

White, R.L. 1985, ApJ, 289, 698

White, R.L., & Becker, R.H. 1995, ApJ, 451, 352

Williams, P.M., van der Hucht, K.A., van der Woerd, H., Wamsteker, W.M., Geballe, T.R., Garmany, C.D., & Pollock, A.M.T. 1987, in: H. Lamers & C.W.H. de Loore (eds.), *Instabilities in Luminous Early Type Stars*, Proc. of a Workshop in honour of Cornelis de Jager (Dordrecht: Reidel), p. 221

Williams, P.M., van der Hucht, K.A., Pollock, A.M.T., Florkowski, D.R., van der Woerd, H., & Wamsteker, W.M. 1990, MNRAS, 243, 662

Williams, P.M., van der Hucht, K.A., Bouchet, P., Spoelstra, T.A.Th., Eenens, P.R.J., Geballe, T.R., Kidger, M.R., & Churchwell, E.B. 1992, MNRAS, 258, 461

Williams, P.M., van der Hucht, K.A., & Spoelstra, T.A.Th. 1994, A&A, 291, 805

Williams, P.M. 1995, in: K.A. van der Hucht & P.M. Williams (eds.), *Wolf-Rayet Stars: Binaries, Colliding Winds, Evolution*, Proc. IAU Symp. No. 163 (Dordrecht:Kluwer), p. 335

Williams, P.M., Dougherty, S.M., Davis, R.J., van der Hucht, K.A., Bode, M.F., & Setia Gunawan, D.Y.A. 1997, MNRAS, 289, 10

Williams, P.M. 2002, in: A.F.J. Moffat & N. St-Louis (eds.), *Interacting Winds from Massive Stars*, ASP-CS, 260, 311

Willis, A.J. 1991, in: K.A. van der Hucht & B. Hidayat (eds.), *Wolf-Rayet Stars and Interrelations with Other Massive Stars in Galaxies*, Proc. IAU Symp. No. 143 (Dordrecht: Kluwer), p. 265

Wright, A.E., & Barlow, M.J. 1975, MNRAS, 170, 41

Zoonematkermani, S., Helfand, D.J., Becker, R.H., White, R.L., & Perley, R.A. 1990, ApJS, 74, 181

Table 1: Selected Wolf-Rayet stars

WR #	other designation (s)	spectral type	d (kpc)	binary status	P (d)	v_∞ ($\mathrm{km\,s^{-1}}$)
4	HD 16523, V493 Per	WC5+?	2.44	SB1, no d.e.l.	2.4	1900
5	HD 17638	WC6	1.91			2100
8	HD 62910	WN7/WCE+?	3.47	SB1	38.4	1590
12	Ve5-5	WN8h+?	5.04	SB1, no d.e.l.	23.9	1100
79a	HD 152408	WN9ha	1.99	VB (6.″9)		935
79b	HD 152386	WN9ha	2.90	VB (0.″55)		1650
80	Wra 1581	WC9d	1.50			1200
81	He3-1316	WC9	1.57			910
82	LS 11	WN7(h)	5.25		2.0	1100
87	LSS 4064	WN7(h)+OB	2.88	a, d.e.l.		1400
88	Thé 1	WC9	2.33			1125
89	AS 223	WN8h+OB	2.88	a, d.e.l., VB (9.″88)		1600
92	HD 157451	WC9	3.84			1100
95	He3-1434	WC9d	2.09			1100
96	LSS 4265	WC9d	3.58			1100
98a	IRAS 17380−3031	WC8-9vd+?	1.9	CWB	565	900[1]
100	HDE 318139	WN7	4.61			1600
103	HD 164270, V4072 Sgr	WC9d+?	2.21	SB1, no d.e.l.	1.8	1100
104	Ve2-45	WC9d+B0.5V	2.3	SB2, VB (0.″975)	243.5	1220
105	Ve2-47	WN9h	1.58			700
106	HDE 313643	WC9d	2.32			1100
113	HD 168206, CV Ser	WC8d+O8-9IV	1.79	SB2	29.7	1700
114	HD 169010	WC5+OB?	2.00	d.e.l.		2000
119	Thé 2	WC9d	3.31			1200
120	Vy1-3	WN7	3.56			1225
121	AS 320	WC9d	1.83			1100
124	209 BAC, QR Sge	WN8h	3.36	SB1?, no d.e.l.	2.7	710
125	IC14-36, V378 Vul	WC7ed+O9III	3.06	SB2	>6600	2900
133	HD 190918, V1676 Cyg	WN5+O9I	2.14	SB2, VB (5.″4)	112.4	1800
142	Sand 5	WO2	0.95			5500[2]
143	HD 195177	WC4+OB?	1.07	d.e.l.		2750
153ab	HD 211853, GP Cep	WN6/WCE +O6I	2.75		6.7	1785
155	HD 214419, CQ Cep	WN6+O9II-Ib	2.75	SB2	1.6	1400
156	AC +60 38562	WN8h+OB?	3.56	d.e.l.	6.5	660

Notes:
Cols.1 and 2: WR catalogue number and any other designation(s);
col. 3: spectral classification; col. 4: heliocentric distance;
col. 5: the binary status, in case of visual binaries (VB), the angular separation is indicated;
col. 6: period;
col. 7: terminal wind velocity.
a: absorption lines present in optical spectrum;
d.e.l.: diluted emission lines
All parameters and values from van der Hucht (2001) except:
1: from Monnier et al. (2002);
2: from Kingsburgh et al. (1995).

Table 2: Optical positions, radio positions, and flux densities of the observed Wolf-Rayet stars

WR #	optical position R.A.(J2000) h m s	optical position Dec.(J2000) ° ′ ″	radio position R.A.(J2000) h m s	radio position Dec.(J2000) ° ′ ″	$S_{3.6cm}$ (mJy)	epoch
			Definite detections			
5	02 52 11.66	+56 56 07.1	02 52 11.62 ± 0.05	+56 56 08.2 ± 0.4	0.20 ± 0.03	2001.9
8	07 44 58.22	−31 54 29.6	07 44 58.26 ± 0.02	−31 54 29.7 ± 0.2	0.46 ± 0.03	2001.8
12	08 44 47.25	−45 58 55.5	08 44 47.33 ± 0.03	−45 58 52.5 ± 0.7	0.51 ± 0.06	2001.8
88	17 18 49.50	−33 57 39.8	17 18 49.67 ± 0.05	−33 57 40.9 ± 0.6	0.26 ± 0.05	2001.8
89	17 19 00.52	−38 48 51.2	17 19 00.49 ± 0.03	−38 48 49.4 ± 0.4	2.0 ± 0.1	2001.7
98a	17 41 12.9	−30 32 29	17 41 13.08 ± 0.03	−30 32 30.0 ± 0.3	0.47 ± 0.05	2001.8
100	17 42 09.77	−32 33 24.7	17 42 09.78 ± 0.02	−32 33 24.9 ± 0.2	0.47 ± 0.04	2001.8
103	18 01 43.14	−32 42 55.2	18 01 43.20 ± 0.05	−32 42 55.7 ± 0.7	0.21 ± 0.04	2001.7
104	18 02 04.07	−23 37 41.2	18 02 04.16 ± 0.02	−23 37 41.0 ± 0.3	0.54 ± 0.06	2001.8
105	18 02 23.46	−23 34 37.7	18 02 23.48 ± 0.01	−23 34 37.3 ± 0.3	5.4 ± 0.1	2001.9
113	18 19 07.36	−11 37 59.2	18 19 07.40 ± 0.01	−11 37 58.9 ± 0.1	0.75 ± 0.04	2001.8
120	18 41 00.88	−04 26 14.3	18 41 00.85 ± 0.03	−04 26 14.6 ± 0.4	0.40 ± 0.04	2001.9
125	19 28 15.57	+19 33 21.1	19 28 15.61 ± 0.01	+19 33 21.6 ± 0.1	1.14 ± 0.03	2001.9
133	20 05 57.33	+35 47 18.2	20 05 57.31 ± 0.02	+35 47 18.6 ± 0.3	0.36 ± 0.03	2001.9
156	23 00 10.13	+60 55 38.4	23 00 10.14 ± 0.01	+60 55 38.4 ± 0.1	1.06 ± 0.03	2001.9
			Probable detections			
79a	16 54 58.51	−41 09 03.1	16 54 58.53 ± 0.05	−41 09 07.8 ± 0.8	0.68 ± 0.13	2001.7
81	17 02 40.39	−45 59 15.5	17 02 40.48 ± 0.06	−45 59 12.9 ± 1.4	0.29 ± 0.07	2001.8
95	17 36 19.76	−33 26 10.9	17 36 19.87 ± 0.05	−33 26 13.4 ± 0.7	0.16 ± 0.04	2001.7
114	18 23 16.39	−13 43 25.8	18 23 16.42 ± 0.04	−13 43 25.9 ± 0.2	0.15 ± 0.04	2001.8
155	22 36 53.96	+56 54 21.0	22 36 53.79 ± 0.10	+56 54 21.5 ± 0.7	0.12 ± 0.03	2001.9
			Undetected sources			
4	02 41 11.68	+56 43 49.7	—	—	< 0.15	2001.9
79b	16 55 06.45	−44 59 21.4	—	—	< 0.20	2001.7
80	16 59 02.2	−45 43 06	—	—	< 0.17	2001.8
82	17 04 04.61	−45 12 15.0	—	—	< 0.23	2001.7
87	17 18 52.89	−38 50 04.5	—	—	<0.24	2001.7
92	17 25 23.15	−43 29 31.9	—	—	< 0.18	2001.8
96	17 36 24.2	−32 54 29	—	—	< 0.16	2001.7
106	18 04 43.66	−21 09 30.7	—	—	< 0.17	2001.8
119	18 39 17.91	−10 05 31.1	—	—	< 0.11	2001.7
121	18 44 13.15	−03 47 57.8	—	—	< 0.17	2001.9
124	19 11 30.88	+16 51 38.2	—	—	< 0.25	2001.9
142	20 21 44.36	+37 22 30.3	—	—	<0.90	2001.9
143	20 28 22.68	+38 37 18.9	—	—	< 0.12	2001.9
153ab	22 18 45.61	+56 07 33.9	—	—	< 0.14	2001.9

Table 3: Radio flux densities of earlier detected Wolf-Rayet stars, compared with our detections

WR #	$S_{21\mathrm{cm}}$	$S_{12.5\mathrm{cm}}$	$S_{6.3\mathrm{cm}}$	$S_{3.6\mathrm{cm}}$	$S_{2.0\mathrm{cm}}$	$S_{1.3\mathrm{cm}}$	spectral index α	references
	present and previous observations (mJy)							
79a			1.1 ± 0.1		2.4 ± 0.1		+0.8	BA89
		1.0 ± 0.1	0.8 ± 0.1	0.9 ± 0.1			−0.0	SC03
				0.7 ± 0.1			V	this study
81			0.3 ± 0.08					AB86
				0.3 ± 0.1				this study
88			<0.42	<0.42				LC97
	<1.29	<0.57						CL99
				0.26 ± 0.05				this study
89			0.6 ± 0.1					AB86
			1.9 ± 0.2	3.0 ± 0.1			+0.8	LC95
	<1.20	<0.90						CL99
				2.0 ± 0.1			V	this study
95			<0.4					AB86
			<0.45	<0.45				LC97
	<1.50	<0.66						CL99
				0.16 ± 0.04				this study
98a	<0.36		0.37 ± 0.07	0.60 ± 0.05	0.64 ± 0.11	0.57 ± 0.10	+0.3	MT02
				0.47 ± 0.05			V	this study
103			≤0.2					AB86
			<0.42	<0.42				LC97
	<0.90	<0.42						CL99
				0.21 ± 0.04				this study
104			<0.4					AB86
			<2.01	<0.39				LC97
	<1.59	<0.99						CL99
	<0.30			0.87 ± 0.06	1.02 ± 0.12	0.94 ± 0.10	+0.1	MT02
				0.54 ± 0.06			V	this study
105			3.6 ± 0.21					AB86
			4.39 ± 0.15	3.8 ± 0.2			−0.3	LC97
	<1.17	<0.69						CL99
				5.4 ± 0.1			V	this study
113			≤0.4					BA82
			<0.80	<0.80				LC97
	<2.25	<0.90						CL99
				0.75 ± 0.04				this study
114			<0.3					AB86
			<0.45	<0.45				LC97
	<1.17	<0.54						CL99
				0.15 ± 0.03				this study
125			1.5 ± 0.09		0.8 ± 0.09		−0.5	AB86
	1.53 ± 0.06		1.18 ± 0.06		0.82 ± 0.10		−0.3	WH92
			0.20 ± 0.04				+0.7 V	WH92
				1.14 ± 0.03				this study
133			<0.3					AB86
				0.36 ± 0.03				this study

Note: V: apparently variable. References: AB86: Abbott et al. (1986); BA82: Bieging et al. (1982); BA89: Bieging et al. (1989); CL99: Chapman et al. (1999); LC95: Leitherer et al. (1995); LC97: Leitherer et al. (1997); MT02: Monnier et al. (2002); SC03: Setia Gunawan et al. (2003a); WH92: Williams et al. (1992).

Table 4: Mass loss rates from 3.6 cm observations of our sample of 34 Wolf-Rayet stars

WR #	d (kpc)	v_∞ ($\mathrm{km\,s^{-1}}$)	μ	Z	γ	$S_{3.6\mathrm{cm}}$ (mJy)	$\log \dot{M}$	$\dot{M}$ ($10^{-5}\,\mathrm{M_\odot\,yr^{-1}}$)	Notes
4	2.44	1900	5.1	1.2	1.0	<0.15	<-4.7	$<$ 2.0	
5	1.91	2100	4.9	1.2	1.0	0.20 ± 0.03	-4.7 ± 0.4	1.8	
8	3.47	1590	1.7	1.0	1.0	0.46 ± 0.03	-4.6 ± 0.2	2.6	
12	5.04	1100	2.6	1.0	1.0	0.51 ± 0.06	-4.3 ± 0.4	5.2	
79a	1.99	935	2.6	1.0	1.0	0.68 ± 0.14	$<-4.9\pm0.2$	$<$ 1.4	NT?
79b	2.9	1650	2.6	1.0	1.0	<0.20	<-4.8	$<$ 1.7	
80	1.5	1200	4.7	1.1	1.1	<0.17	<-5.2	$<$ 0.6	
81	1.57	910	4.7	1.1	1.1	0.29 ± 0.07	-5.1 ± 0.4	0.8	
82	5.25	1100	1.7	1.0	1.0	<0.23	<-4.7	$<$ 1.9	
87	2.88	1400	1.8	1.0	1.0	<0.24	<-4.9	$<$ 1.2	
88	2.33	1125	4.7	1.1	1.1	0.26 ± 0.05	-4.8 ± 0.4	1.6	
89	2.88	1600	1.5	1.0	1.0	$2.0\ \ \pm0.1$	-4.3 ± 0.2	5.2	NT?
92	3.84	1100	4.7	1.1	1.1	<0.18	<-4.6	$<$ 2.5	
95	2.09	1100	4.7	1.1	1.1	0.16 ± 0.04	-5.0 ± 0.2	1.0	
96	3.58	1100	4.7	1.1	1.1	<0.16	<-4.7	$<$ 2.1	
98a	1.9	2000	4.7	1.1	1.1	0.47 ± 0.05	$<-4.8\pm0.2$	$<$ 1.5	NT
100	4.61	1600	4.0	1.0	1.0	0.47 ± 0.04	-4.0 ± 0.4	9.5	
103	2.21	1100	4.7	1.1	1.1	0.21 ± 0.04	-4.9 ± 0.4	1.2	
104	2.3	1220	4.7	1.1	1.1	0.54 ± 0.06	$<-4.5\pm0.2$	$<$ 2.9	NT
105	1.58	700	2.6	1.0	1.0	$5.4\ \ \pm0.1$	$<-4.5\pm0.4$	$<$ 3.4	NT
106	2.32	1100	4.7	1.1	1.1	<0.17	<-5.0	$<$ 1.1	
113	1.79	1700	4.7	1.1	1.1	0.75 ± 0.04	-4.4 ± 0.2	3.6	
114	2.0	2000	4.9	1.2	1.1	0.15 ± 0.04	-4.8 ± 0.2	1.5	
119	3.31	1200	4.7	1.1	1.1	<0.11	<-4.8	$<$ 1.5	
120	3.56	1225	4.0	1.0	1.0	0.40 ± 0.04	-4.4 ± 0.4	4.4	
121	1.83	1100	4.7	1.1	1.1	<0.17	<-5.1	$<$ 0.8	
124	3.36	710	3.7	1.0	1.0	<0.25	<-4.9	$<$ 1.3	
125	3.06	2900	4.7	1.2	1.1	1.14 ± 0.03	$<-3.8\pm0.4$	$<$17.1	NT
133	2.14	1800	4.0	1.1	1.1	0.36 ± 0.03	-4.6 ± 0.2	2.8	
142	0.95	5500	5.1	1.2	1.1	<0.77	<-4.3	$<$ 4.5	
143	1.07	2750	5.1	1.2	1.0	<0.12	<-5.2	$<$ 0.7	
153ab	2.75	1785	4.0	1.0	1.0	<0.14	<-4.7	$<$ 2.0	
155	2.75	1400	4.0	1.0	1.0	0.12 ± 0.03	-4.9 ± 0.2	1.4	
156	3.56	660	3.3	1.0	1.0	1.06 ± 0.03	-4.4 ± 0.2	4.0	

Fig. 1.— Contour image for WR 5. The cross marks the optical position of the WR star, and the ellipse in one of the corners, the synthesized beam. We note that the extend of the cross does not represent the uncertainty in the stellar position. Contour lines are –3 (dashed contour), 3, 4, 5, 6 and 7σ ($1\sigma = 0.025$ mJy beam^{-1}).

Fig. 2.— Contour image for WR 8. Contour lines are –3 (dashed contour), 3, 4, 5, 6, 8, 10, 12 and 14σ ($1\sigma = 0.030$ mJy beam^{-1}).

Fig. 3.— Contour image for WR 12. Contour lines are –3 (dashed contour), 3, 4, 5, 6, 7, 8 and 9σ ($1\sigma = 0.055$ mJy beam^{-1}).

Fig. 4.— Contour image for WR 79a. Contour lines are –3 (dashed contour), 3 and 4σ ($1\sigma = 0.125$ mJy beam^{-1}).

Fig. 5.— Contour image for WR 81. Contour lines are –3 (dashed contour) and 3σ ($1\sigma = 0.065$ mJy beam^{-1}).

Fig. 6.— Contour image for WR 88. Contour lines are –3 (dashed contour), 3, 4 and 5σ ($1\sigma = 0.050$ mJy beam^{-1}).

Fig. 7.— Contour image for WR 89. Contour lines are –3 (dashed contour), 3, 4, 5, 6, 7, 9, 11 and 13σ ($1\sigma = 0.130$ mJy beam^{-1}).

Fig. 8.— Contour image for WR 95. Contour lines are –3 (dashed contour) and 3σ ($1\sigma = 0.040$ mJy beam^{-1}).

Fig. 9.— Contour image for WR 98a. Contour lines are –3 (dashed contour), 3, 4, 5, 6 and 7σ ($1\sigma = 0.050$ mJy beam^{-1}).

Fig. 10.— Contour image for WR 100. Contour lines are –3 (dashed contour), 3, 4, 5, 6, 7, 8, 10 and 12σ ($1\sigma = 0.040$ mJy beam^{-1}).

Fig. 11.— Contour image for WR 103. Contour lines are –3 (dashed contour), 3 and 4σ ($1\sigma = 0.040$ mJy beam^{-1}).

Fig. 12.— Contour image for WR 104. Contour lines are –3 (dashed contour), 3, 4, 5, 6 and 7σ ($1\sigma = 0.060$ mJy beam^{-1}).

Fig. 13.— Contour image for WR 105. Contour lines are –3 (dashed contour), 3, 6, 12, 24, 36, 48, and 60σ ($1\sigma = 0.080$ mJy beam^{-1}).

Fig. 14.— Contour image for WR 113. Contour lines are –3 (dashed contour), 3, 6, 9, 12, 15 and 17σ ($1\sigma = 0.040$ mJy beam^{-1}).

Fig. 15.— Contour image for WR 114. Contour lines are –3 (dashed contour) and 3σ ($1\sigma = 0.040$ mJy beam^{-1}).

Fig. 16.— Contour image for WR 120. Contour lines are –3 (dashed contour), 3, 4, 5, 6, 7, 8, 9 and 10σ ($1\sigma = 0.035$ mJy beam^{-1}).

Fig. 17.— Contour image for WR 125. Contour lines are –3 (dashed contour), 3, 6, 9, 12, 15, 18, 24, 30 and 35σ ($1\sigma = 0.030$ mJy beam^{-1}).

Fig. 18.— Contour image for WR 133. *Upper panel:* Contour lines are –3 (dashed contour), 3, 4, 6, 8, 10, 12 and 14σ ($1\sigma = 0.025$ mJy beam^{-1}). *Lower panel:* Overlay of the DSS2 red image of WR 133 (gray scale, in arbitrary units) and the radio continuum emission at 3.6 cm.

Fig. 19.— Contour image for WR 155. Contour lines are –3 (dashed contour), 3 and 4σ ($1\sigma = 0.025$ mJy beam^{-1}).

Fig. 20.— Contour image for WR 156. Contour lines are –3 (dashed contour), 3, 6, 9, 12, 15, 18, 24 and 30σ ($1\sigma = 0.030$ mJy beam^{-1}).

Fig. 21.— WR mass loss rates ($\log \dot{M}$, where $\dot{M}$ is in units of $M_\odot\,yr^{-1}$) from radio observations *versus* spectral subtype. *Upper panel:* Mass loss rates derived from the present VLA survey. *Bona fide* mass loss rates values corresponding to detected sources are indicated as filled circles. Bar errors are included. Open circles indicate upper limits corresponding to both detected sources with variable flux density and undetected sources. *Lower panel:* Mass loss rates derived for the VLA and ATCA target stars. Open and filled circles have the same meaning as in the upper panel.

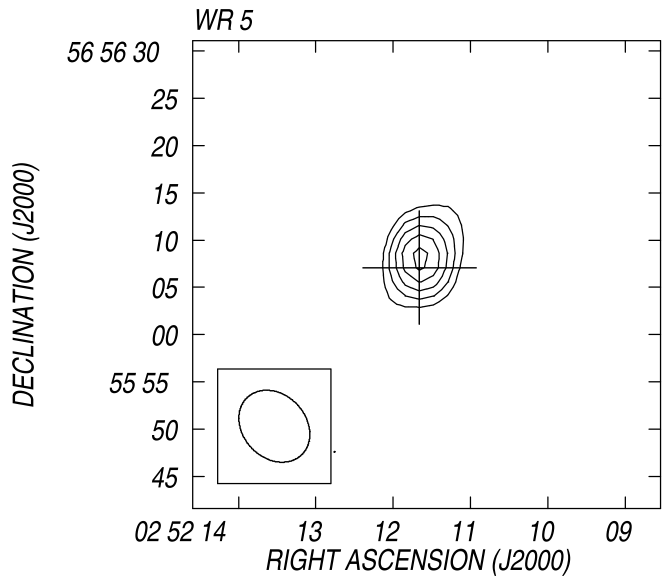
WR 5
56 56 30
25
20
15
10
05
00
55 55
50
45
DECLINATION (J2000)
02 52 14
13
12
11
10
09
RIGHT ASCENSION (J2000)

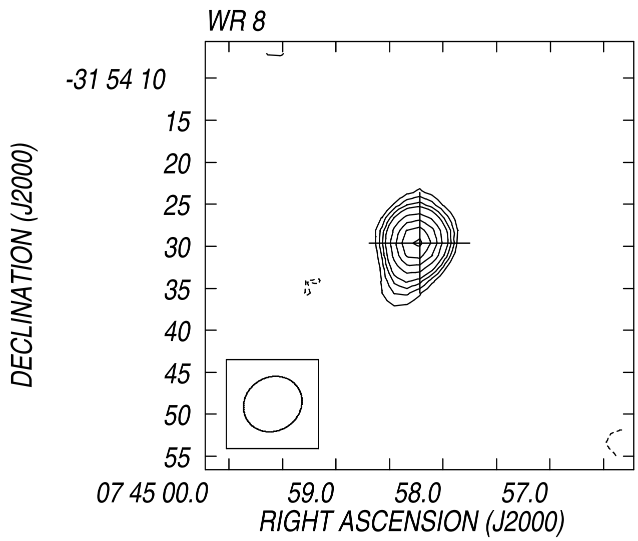

WR 8
-31 54 10
15
20
25
30
35
40
45
50
55
07 45 00.0
59.0
58.0
57.0
DECLINATION (J2000)
RIGHT ASCENSION (J2000)

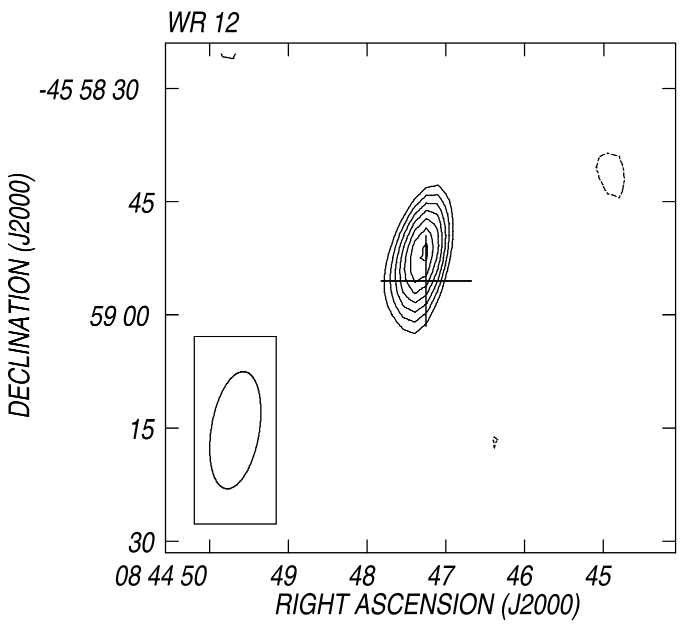
WR 12
-45 58 30
45
59 00
15
30
08 44 50
49
48
47
46
45
DECLINATION (J2000)
RIGHT ASCENSION (J2000)

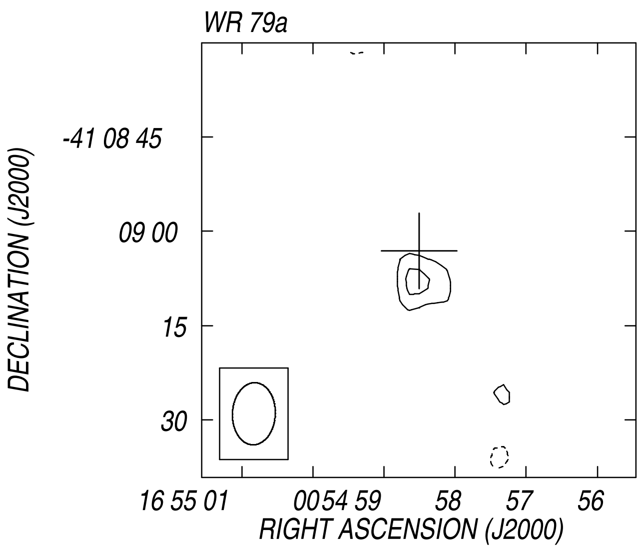
WR 79a
-41 08 45
09 00
15
30
DECLINATION (J2000)
16 55 01
00 54 59
58
57
56
RIGHT ASCENSION (J2000)

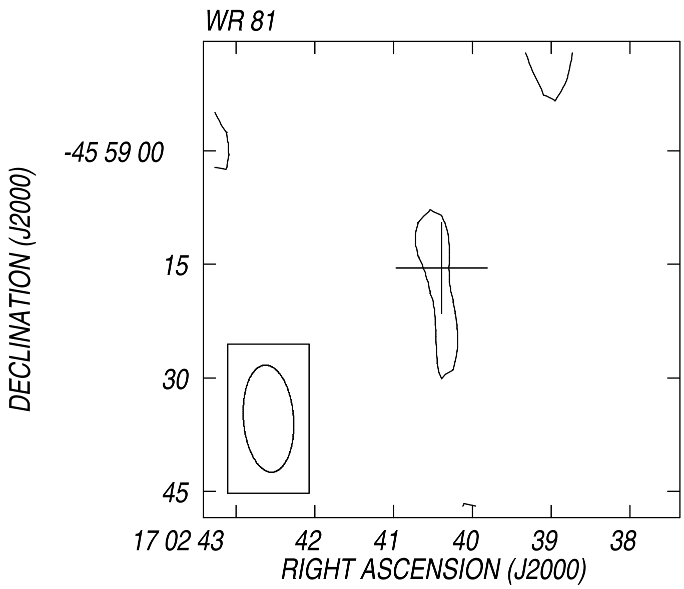

WR 81
-45 59 00
15
30
45
DECLINATION (J2000)
17 02 43
42
41
40
39
38
RIGHT ASCENSION (J2000)

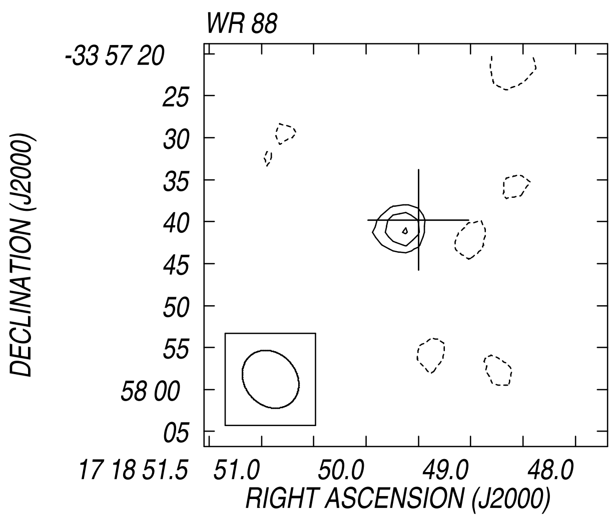
WR 88
-33 57 20
25
30
35
40
45
50
55
58 00
05
DECLINATION (J2000)
17 18 51.5
51.0
50.0
49.0
48.0
RIGHT ASCENSION (J2000)

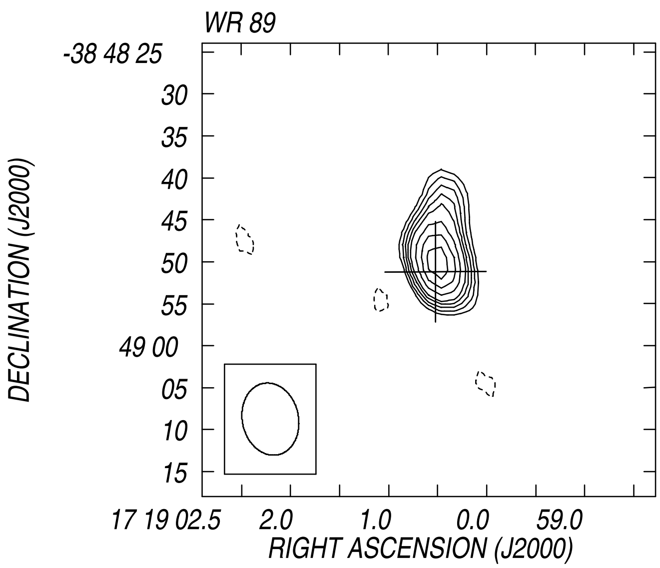

WR 89
-38 48 25
30
35
40
45
50
55
49 00
05
10
15
DECLINATION (J2000)
17 19 02.5
2.0
1.0
0.0
59.0
RIGHT ASCENSION (J2000)

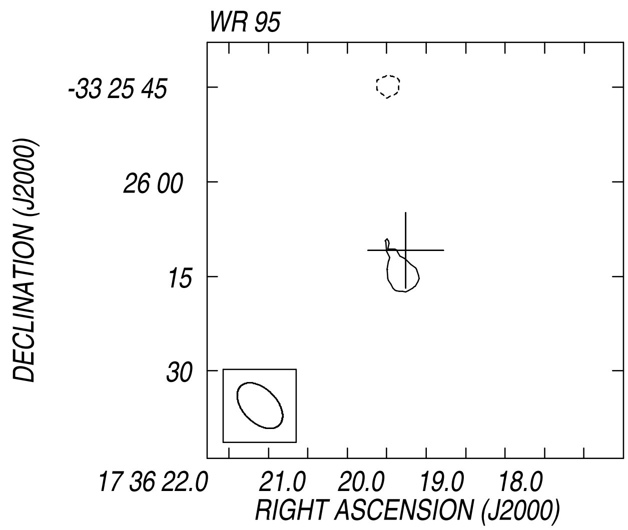
WR 95
-33 25 45
26 00
15
30
DECLINATION (J2000)
17 36 22.0
21.0
20.0
19.0
18.0
RIGHT ASCENSION (J2000)

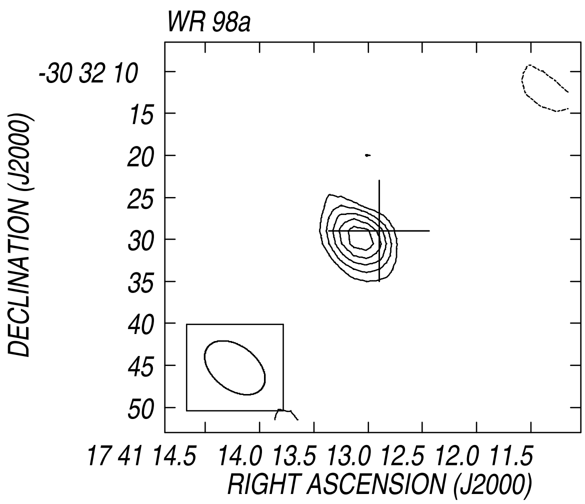
WR 98a
-30 32 10
15
20
25
30
35
40
45
50
DECLINATION (J2000)
17 41 14.5
14.0
13.5
13.0
12.5
12.0
11.5
RIGHT ASCENSION (J2000)

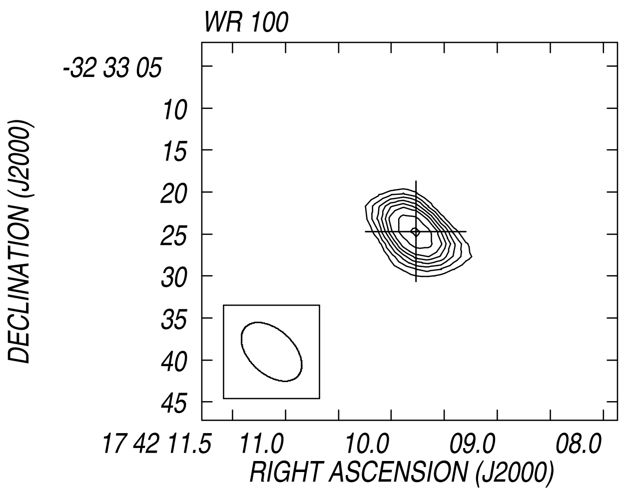

WR 100
-32 33 05
10
15
20
25
30
35
40
45
DECLINATION (J2000)
17 42 11.5
11.0
10.0
09.0
08.0
RIGHT ASCENSION (J2000)

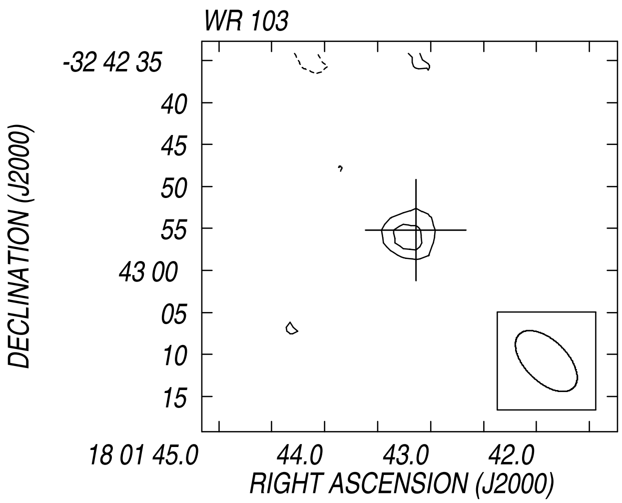
WR 103
-32 42 35
40
45
50
55
43 00
05
10
15
DECLINATION (J2000)
18 01 45.0
44.0
43.0
42.0
RIGHT ASCENSION (J2000)

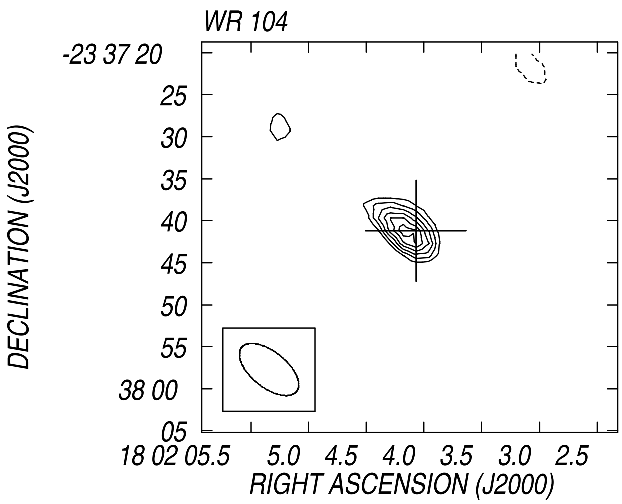

WR 104
-23 37 20
25
30
35
40
45
50
55
38 00
05
18 02 05.5
5.0
4.5
4.0
3.5
3.0
2.5
RIGHT ASCENSION (J2000)
DECLINATION (J2000)

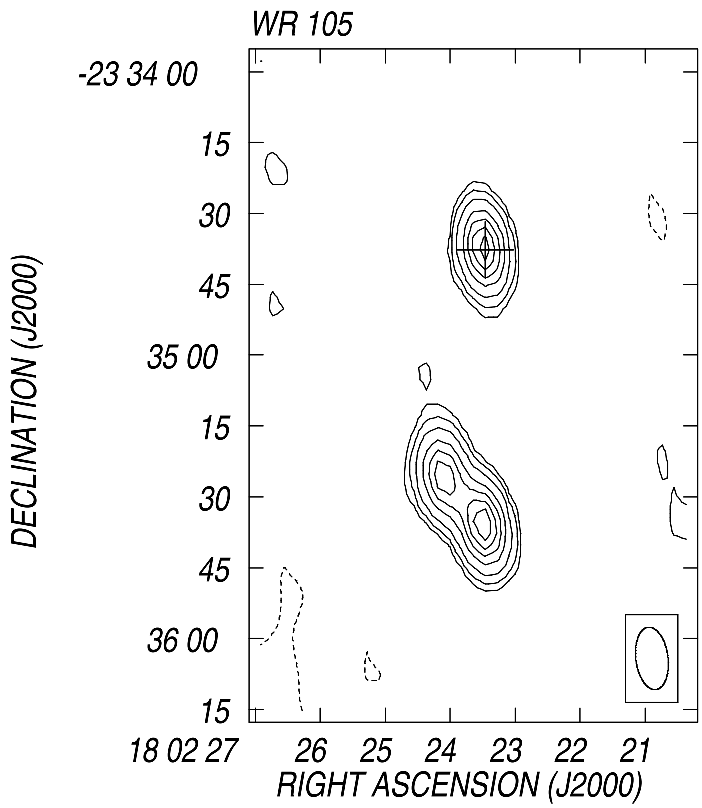
WR 105
-23 34 00
15
30
45
35 00
15
30
45
36 00
15
DECLINATION (J2000)
18 02 27
26
25
24
23
22
21
RIGHT ASCENSION (J2000)

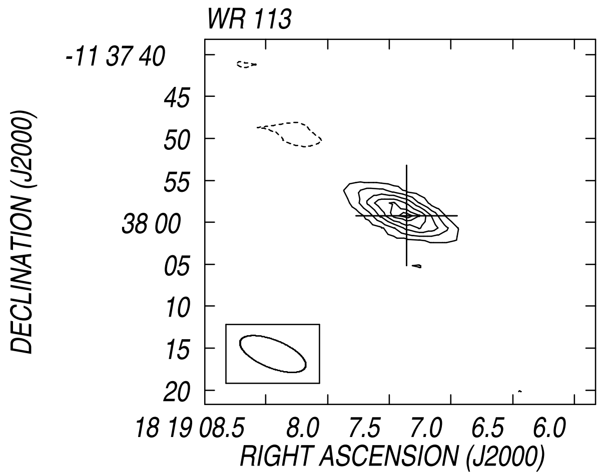
WR 113
-11 37 40
45
50
55
38 00
05
10
15
20
DECLINATION (J2000)
18 19 08.5
8.0
7.5
7.0
6.5
6.0
RIGHT ASCENSION (J2000)

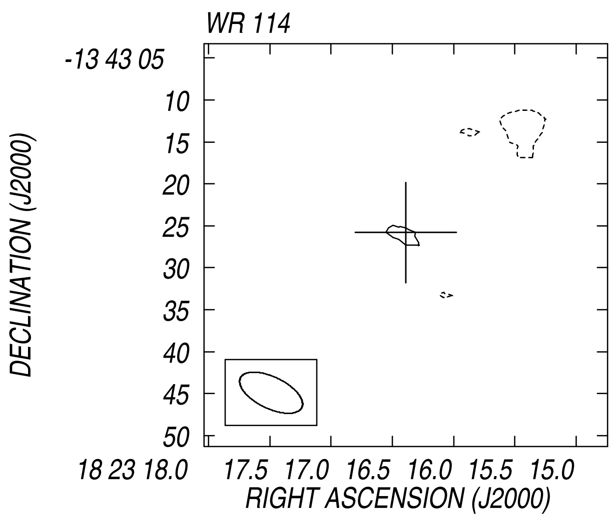
WR 114
-13 43 05
10
15
20
25
30
35
40
45
50
18 23 18.0
17.5 17.0 16.5 16.0 15.5 15.0
RIGHT ASCENSION (J2000)
DECLINATION (J2000)

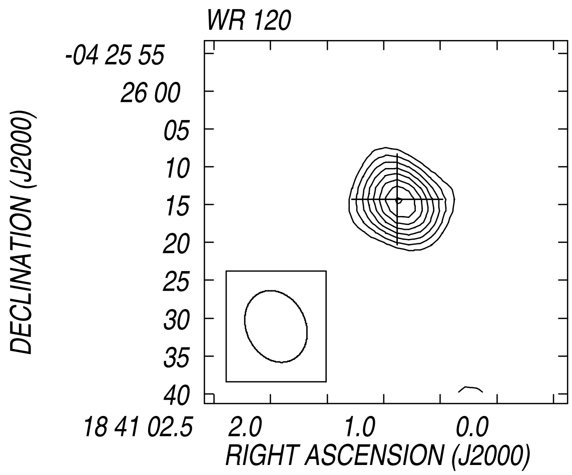
WR 120
-04 25 55
26 00
05
10
15
20
25
30
35
40
DECLINATION (J2000)
18 41 02.5
2.0
1.0
0.0
RIGHT ASCENSION (J2000)

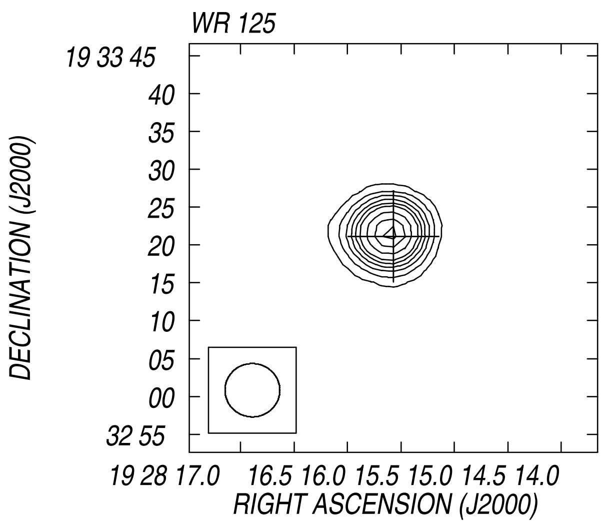
WR 125
19 33 45
40
35
30
25
20
15
10
05
00
32 55
DECLINATION (J2000)
19 28 17.0
16.5
16.0
15.5
15.0
14.5
14.0
RIGHT ASCENSION (J2000)

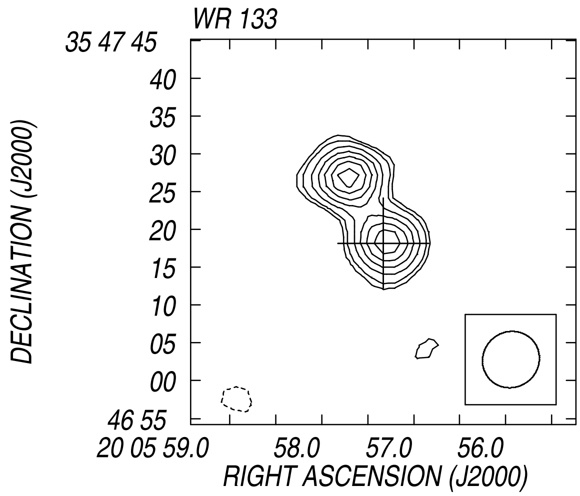

WR 133
35 47 45
40
35
30
25
20
15
10
05
00
46 55
DECLINATION (J2000)
20 05 59.0
58.0
57.0
56.0
RIGHT ASCENSION (J2000)

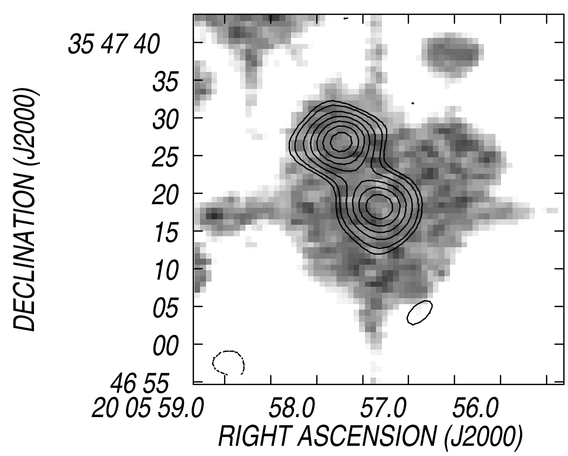

35 47 40
35
30
25
20
15
10
05
00
46 55
DECLINATION (J2000)
20 05 59.0
58.0
57.0
56.0
RIGHT ASCENSION (J2000)

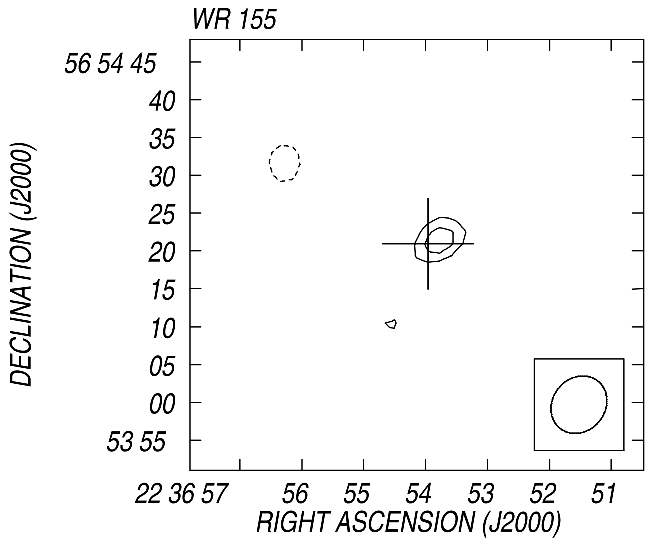
WR 155
56 54 45
40
35
30
25
20
15
10
05
00
53 55
DECLINATION (J2000)
22 36 57
56
55
54
53
52
51
RIGHT ASCENSION (J2000)

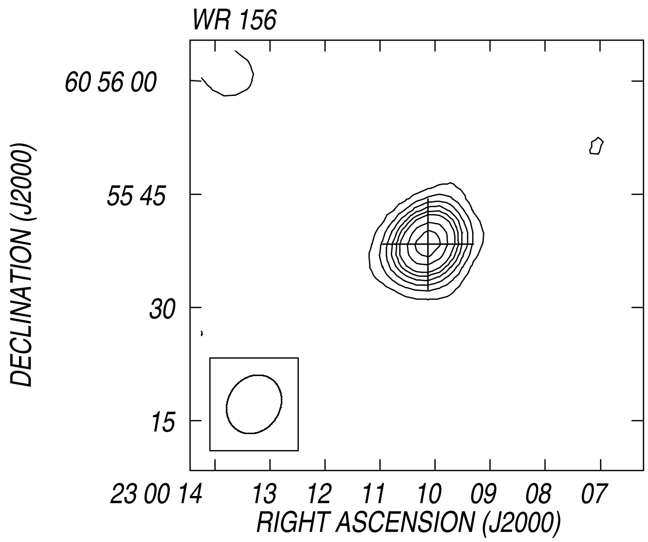
WR 156
60 56 00
55 45
30
15
DECLINATION (J2000)
23 00 14
13
12
11
10
09
08
07
RIGHT ASCENSION (J2000)

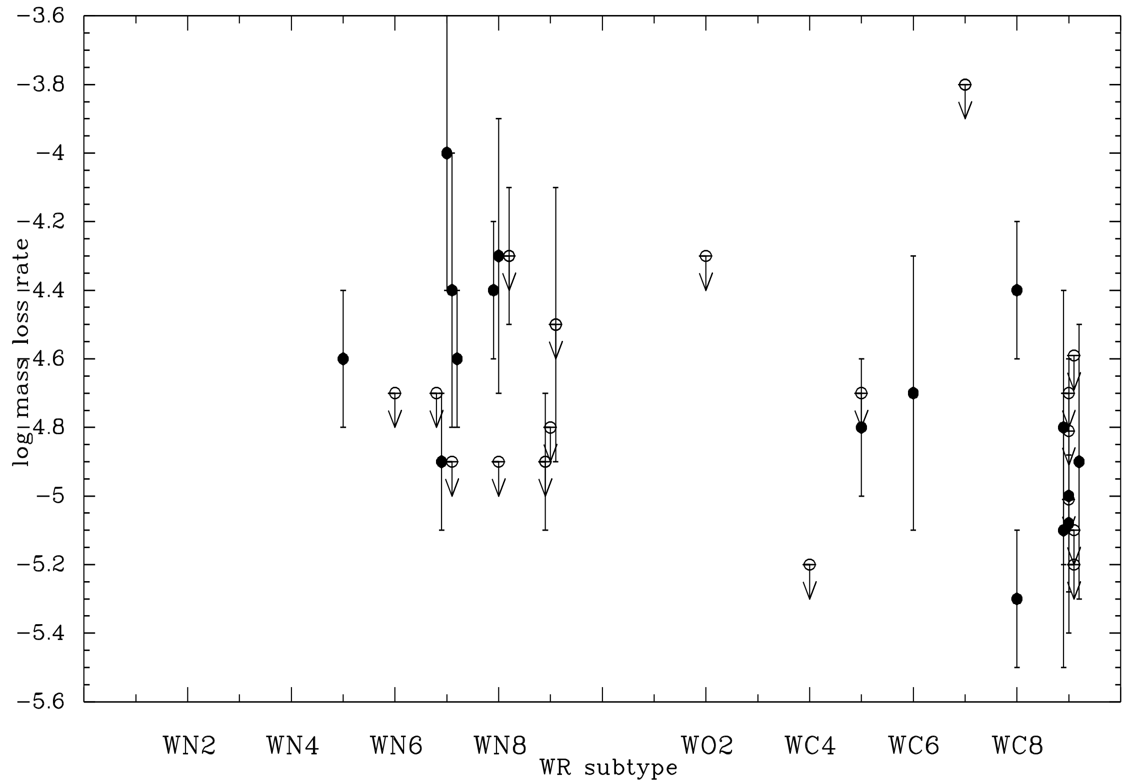

log mass loss rate
WR subtype
WN2
WN4
WN6
WN8
WO2
WC4
WC6
WC8

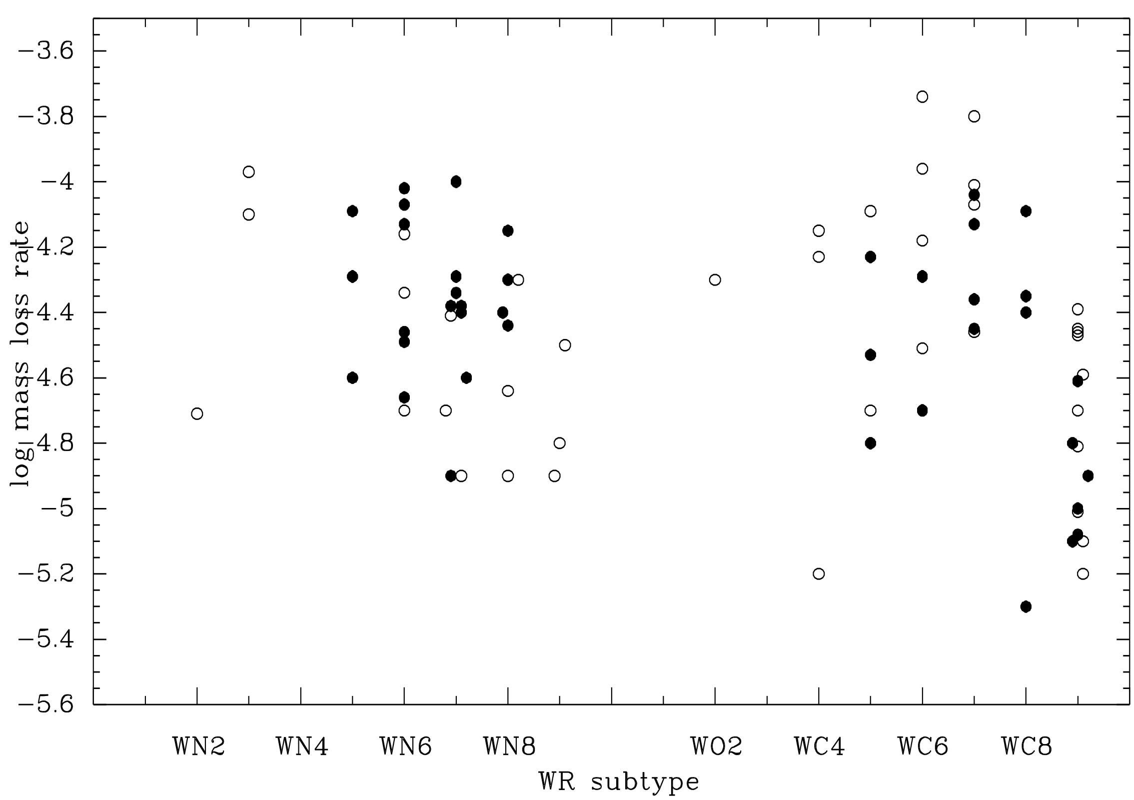

log mass loss rate
WR subtype
WN2
WN4
WN6
WN8
WO2
WC4
WC6
WC8